Influence of PECVD Deposition Power and Pressure on Phosphorus-Doped Polysilicon Passivating Contacts

Wenhao Chen, Josua Stuckelberger, Wenjie Wang, Sieu Pheng Phang, Di Kang, Christian Samundsett, Daniel MacDonald, Andres Cuevas, Lang Zhou, Yimao Wan, and Di Yan

***Abstract*—Passivating contacts for silicon solar cells can be fabricated by depositing a layer of intrinsic amorphous silicon (a-Si) by the plasma-enhanced chemical vapor deposition (PECVD) onto an oxidized silicon wafer, followed by a thermal $POCl_3$ diffusion process. This article describes the influence of the main PECVD parameters, power and pressure, on the electrical performance of such phosphorus-doped polysilicon (doped-Si/SiO_x) passivating contacts. We characterize their properties in terms of the passivation quality and carrier selectivity for different PECVD powers and pressures. The deposition power settings from 350 to 800 W are tried, the highest iV_{oc} value of 721 mV is achieved at a power of 500 W. The higher deposition powers ($\geq$650 W) lead to blistering issues and possible interface damage, while a lower deposition power (350 W) leads to incomplete decomposition of the precursor gas, resulting in a lower passivation quality. Meanwhile, the power has a marginal impact on the contact resistivity. On the other hand, the deposition pressure has only a slight impact on the passivation quality, while significant changes are observed on the contact resistivity. A lower pressure (0.1 mbar) leads to a higher contact resistivity, while the low and consistent contact resistivity values of 5.8 m$\Omega\cdot$cm^2 are obtained at the pressures above 0.2 mbar.**

***Index Terms*—Doped silicon, passivating contact, plasma-enhanced chemical vapor deposition (PECVD), power, poly-Si, pressure, silicon solar cell, Topcon.**

I. Introduction

EXCELLENT surface passivation and carrier selectivity can be obtained using carrier-selective passivating contacts based on an ultrathin silicon oxide (SiO_X) layer capped with a highly doped silicon layer (doped-Si) [1]–[15]. Over the last few years, this passivating contact structure has been implemented into the silicon solar cells [16]–[20] that have achieved conversion efficiencies as high as 26.1% [21]. The approach based on the nitric acid oxidation of the silicon wafer, a plasma-enhanced chemical vapor deposition (PECVD) of the intrinsic amorphous silicon (a-Si) and a subsequent thermal diffusion of boron or phosphorus, has been shown to be an effective way of making high-performance passivating contacts [22], [23] and it has been proved to be effective in the application of high-efficiency cells [17]. As presented in the literature, the properties of the as-deposited intrinsic a-Si films have a significant impact on the final electrical performance of the passivating contact [24], [25]. Our previous studies [26] found that a higher PECVD deposition temperature tends to form the intrinsic silicon films with a higher degree of crystallinity. This leads to large changes in the concentration of the Si-H and Si-O bonds in the as-deposited a-Si films and their subsequent heavily doped silicon (doped-Si) layers. Consequently, these structural variations affect both their passivation qualities and contact resistivity values after thermal diffusion processes. Apart from the deposition temperature, other deposition parameters, such as pressure, plasma power, and gas flow ratios, also affect the silicon film properties [27]–[30].

The experimental studies of the SiN_x films deposited by the microwave (μW) and radio frequency (RF) combined PECVD equipment indicate that temperature, plasma power, and pressure are the main factors affecting the properties of SiN_x [31]. The plasma power and deposition pressure have a strong impact on the gas-phase dissociation rate and the shape of the electron distribution function in the plasma [32], [33]. The plasma power is primarily dominated by the μW plasma in a μW/RF PECVD reactor because the ion density in a μW plasma is more than one order of the magnitude higher than that in an RF plasma [33]. In this article, the influence of PECVD μW power and pressure on the characteristics of both as-deposited a-Si and subsequently diffused doped-Si films are studied by examining their crystallinity, film density, and hydrogen concentration. This is complemented with a study of their impact on the electrical performance of the final structure, which helps us to optimize the PECVD intrinsic a-Si deposition processes for the fabrication of high-performing passivating contacts.

Manuscript received March 9, 2020; revised May 2, 2020; accepted June 1, 2020. Date of publication June 22, 2020; date of current version August 20, 2020. The work was supported in part by the Australian Renewable Energy Agency via the Australian Centre for Advanced Photovoltaics and in part by the graduate school of Nanchang University. *(Corresponding authors: Lang Zhou; Di Yan.)*

Wenhao Chen and Lang Zhou are with the Institute of Photovoltaics, Nanchang University, Nanchang 330031, China (e-mail: wenhao.chen@email.ncu.edu.cn; lzhou@ncu.edu.cn).

Josua Stuckelberger, Wenjie Wang, Sieu Pheng Phang, Di Kang, Christian Samundsett, Daniel MacDonald, Andres Cuevas, Yimao Wan, and Di Yan are with the Research School of Electrical, Energy and Materials Engineering, The Australian National University, Canberra, ACT 0200, Australia (e-mail: josua.stuckelberger@anu.edu.au; wenjie.wang@anu.edu.au; pheng.phang@anu.edu.au; di.kang@anu.edu.au; chris.samundsett@anu.edu.au; daniel.macdonald@anu.edu.au; andres.cuevas@anu.edu.au; yimao.wan@anu.edu.au; di.yan@anu.edu.au).

Color versions of one or more of the figures in this article are available online at https://ieeexplore.ieee.org.

Digital Object Identifier 10.1109/JPHOTOV.2020.3001166

II. Experimental Methods

The quarters of 4 in n-type Czochralski (Cz) (100) silicon wafers (10 Ω·cm, 300 μm thick) with the symmetrical passivating contact structures are used to measure the properties and passivation qualities. The contact resistivity ρ_c is obtained from the Cox and Strack method [34] using the n-type 1.1 Ω·cm Cz silicon wafers with single-sided passivating contact structures. The contact resistivity data is extracted from the *I–V* curves obtained from a Keithley 2420 source meter. The accuracy of this method can be affected by the bulk resistivity and thickness variations. We set the bulk resistivity range of $1.1 \pm 0.5\ \Omega$ and thickness range of $260 \pm 3\ \mu$m to estimate the uncertainty. All the samples have been chemically etched to remove saw damages before being cleaned in standard RCA solutions. Subsequently, an ultrathin silicon oxide with a thickness of ∼1.4 nm is formed after 30 min in a 68 wt% hot nitric acid (∼90 °C) solution [18], [35], [36].

The intrinsic a-Si films are deposited by PECVD (AK-400, Roth & Rau, μW/RF dual-mode, and SiH_4 and Ar as precursor gasses) at a substrate temperature of 300 °C. Various powers (350, 500, 650, and 800 W) and pressures (0.1, 0.2, and 0.4 mbar) are explored to deposit intrinsic a-Si films. The deposition condition with a 500 W μW power and 0.2 mbar pressure is used as a reference in this work. The film thickness is measured by spectroscopic ellipsometry (JA Woollam M2000D). For a fixed deposition time of 150 s, a-Si film thicknesses are 52.6 nm, 55 nm, 59 nm, and 64.8 nm for μW power of 350 W, 500 W, 650 W, and 800 W, respectively. The deposition rate increases with increasing power, possibly because the high-power plasma decomposes the precursor gas more effectively [31]. On the other hand, the trend is opposite when increasing the pressure. A probable reason is that the precursor gas particles are packed more closely together at a higher pressure, and thus the probability of their colliding onto one another also increases [37]. Such collisions would result in the polymerization of SiH_4 towards a higher order silane, which does not contribute to the growing film [38]. In this case, we increase the deposition time by 20 s for the high-pressure condition (0.4 mbar) to simplify the analysis by maintaining the a-Si layer thickness approximately constant, ending up with 56 nm, 55 nm, and 55.7 nm for 0.1 mbar, 0.2 mbar, and 0.4 mbar, respectively.

After the PECVD deposition, both passivation and contact resistivity test samples are doped by $POCl_3$ thermal diffusion at a temperature of 800 °C. Subsequently, the phosphorus-silica glasses are removed by 2% HF solution and a 400 °C forming gas annealing is performed for the hydrogenation. Their passivation qualities are measured by the transient photoconductance decay (PCD) [39] at the room temperature, qualified by the implied open circuit (iV_{oc}). For the contact resistivity samples, the aluminum circular contacts are formed on the side with the doped-Si layers and full-area aluminum contact is fabricated on the opposite side.

Various characterization tools, such as a grazing-incidence X-ray diffraction (GIXRD, XPert Pro MPD, Panalytical, Cu anode, 40 mA current, 45 kV acceleration voltage, and $\omega = 1°$) and a Fourier-transform infrared spectroscopy (FTIR, Bruker VERTEX 80v), are used to evaluate the material properties of the a-Si and doped-Si films. The crystallization degree of doped-Si is assessed by the Raman spectroscopy (Horiba T6400 equipped with a confocal microscope, 532 nm laser). With a 532 nm laser, the sampling depth ranges between 100–200 nm [40], [41]. This means the final spectrum contains strong signals from the silicon substrate. However, based on the fact that the thickness of the measured films is very similar, a rough crystallization comparison can be made, in relative terms. An electrochemical capacitance–voltage instrument (ECV, WEP Wafer Profile CVP21) is used to obtain the concentration of electrically active phosphorus dopants in the structure of the doped-Si/SiO_x/Si.

III. Results and Discussion

A. Influence of Deposition Power

Fig. 1(a) shows the iV_{oc} of the as-deposited a-Si/SiO_x as a function of power. The a-Si deposited by the 350 W power has the lowest iV_{oc}. It is worth mentioning that after the 350 W power PECVD deposition, some yellow powder is observed on the surface of the silicon wafers. We speculate that the lower deposition power leads to incomplete decomposition of the precursor gas, which results in a low passivation quality and some residual powders. On the other hand, a higher iV_{oc} for the a-Si/SiO_x structure is observed at a higher PECVD deposition power (>650 W), since more effective decomposition of the gas and a higher hydrogen concentration is expected at higher power conditions [42]. Based on the FTIR results, as shown in Fig. 1(b), the hydrogen concentration in the as-deposited intrinsic a-Si films [dotted line in Fig. 1(b)] can be calculated by the absorption coefficient peaks at the wavenumbers of ∼2000 cm^{-1} and ∼2100 cm^{-1}, which represent the stretching mode of the monohydride (Si-H) and dihydride ($Si-H_2$) bands, respectively [43], [44]. The hydrogen concentrations corresponding to different deposition powers (350, 500, 650, and 800 W) are approximately 1.05×10^{22}, 1.0×10^{22}, 1.35×10^{22}, and 1.2×10^{22} cm^{-3}. This indicates that a high power (≥650 W) leads to a slightly higher hydrogen concentration. Furthermore, the literature [45], [46] indicates that a higher hydrogen concentration is present at the interface between the a-Si and substrate than inside the a-Si films. A higher interfacial hydrogen concentration results in a better passivation quality [47] before the thermal diffusion. However, the excessive hydrogen present at the a-Si/SiO_x interface may weaken the adhesion between the a-Si films and interfacial oxide layers [48]. Serious blistering issues are found in the sample with the high-power deposited a-Si films (at 650 and 800 W) before and after the thermal diffusion step, as indicated in Fig. 2(a) and (b), which may cause the deterioration of the passivation quality. In addition, a high deposition power may also lead to more plasma damage on the SiO_x layers, which should also be an adverse factor for a good passivation quality.

After the thermal $POCl_3$ diffusion, the a-Si/SiO_x structures are transformed into doped-Si/SiO_x structures. Their iV_{oc} values as a function of the deposition power are indicated in Fig. 1(a). The optimized iV_{oc} of 721 mV is achieved at a deposition power

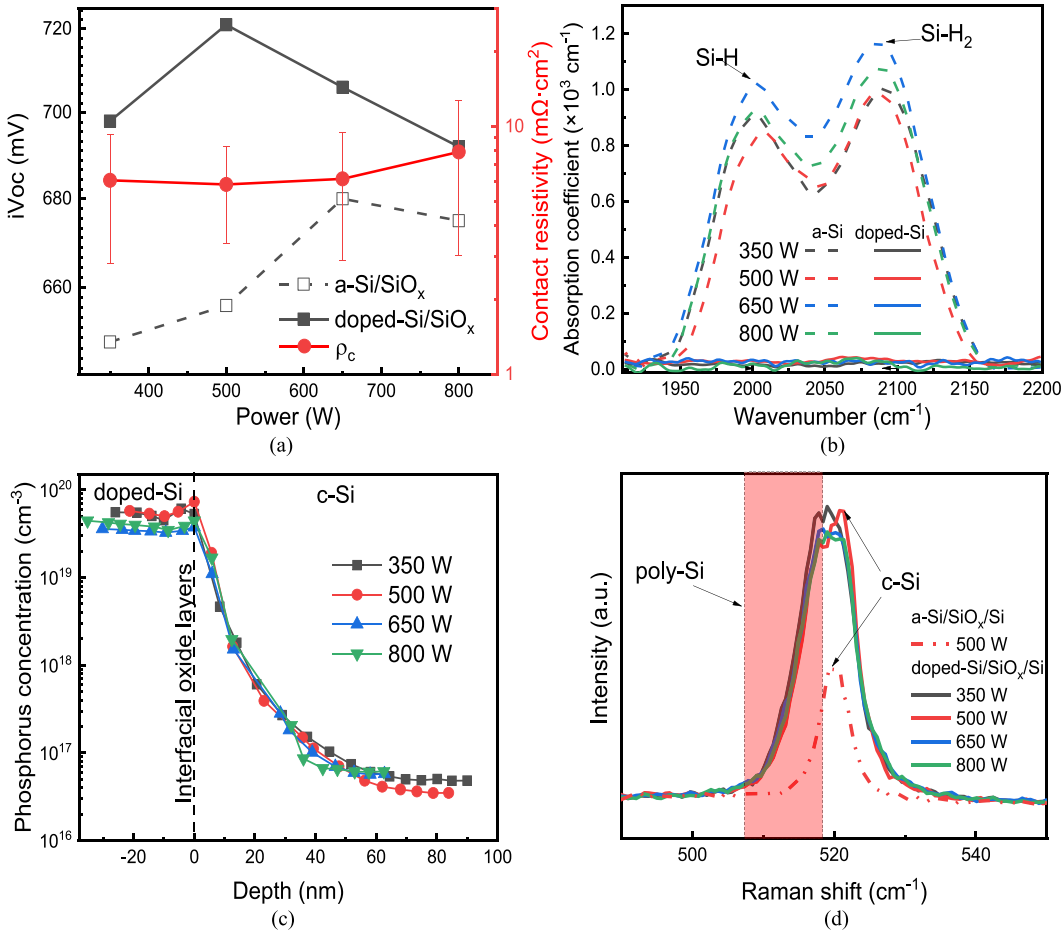

Fig. 1. Comparison of the electrical and material properties of a-Si (dashed lines, open symbols) deposited by different PECVD deposition powers and of the corresponding doped-Si (solid lines, filled symbols). (a) Implied open-circuit voltage (black) and contact resistivity (red). (b) Detail view for the FTIR absorption coefficient peaks of Si-H and Si-H_2. (c) ECV doping profile of the final doped-Si/SiO_x/Si structures. The location of the interfacial oxide layer is set as zero. (d) Raman spectra of 500 W a-Si/SiO_x/Si and different power doped-Si/SiO_x/Si structures. The highlighted area is the range corresponding to the polycrystalline or microcrystalline phases' contributions.

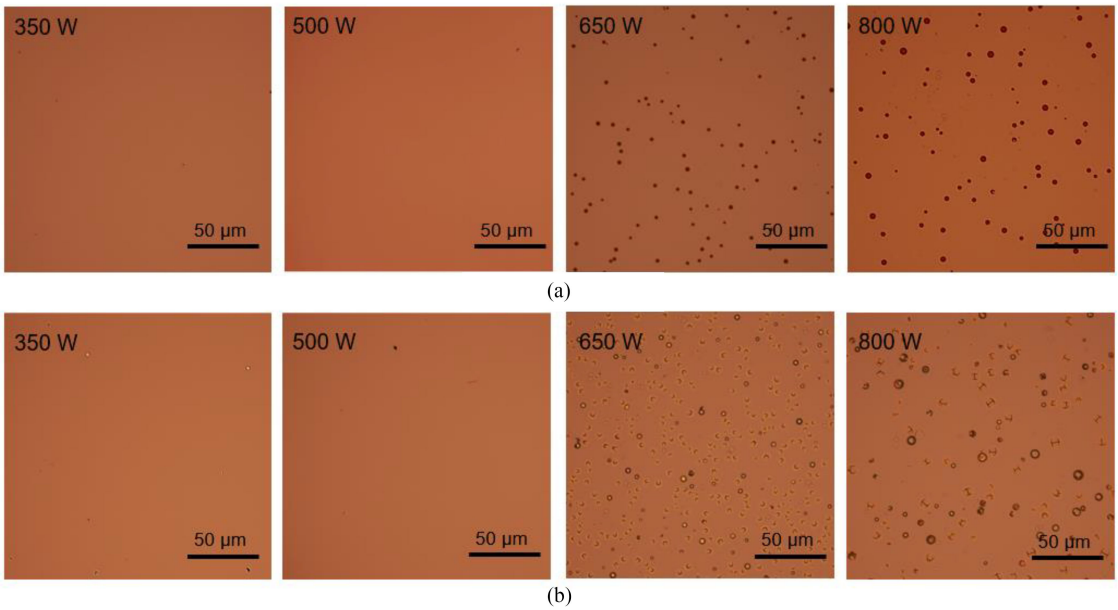

Fig. 2. Surface morphologies of (a) a-Si films and (b) doped-Si layers deposited by different PECVD deposition powers.

of 500 W. A low iV_{oc} of the final passivating contact structure is observed at a low deposition power (350 W). This could be explained by the fact that at a lower deposition power, it is harder to decompose SiH_4 effectively. The low iV_{oc} at high power (650 and 800 W) relates to the blistering issues that become more serious after the thermal diffusion step [as shown in Fig. 2(b)]. During the thermal diffusion, a rapid release of hydrogen happened for all samples, which is confirmed by FTIR and shown as solid lines in Fig. 1(b). Their hydrogen concentration can be treated as zero after the diffusion. Thus, additional blistering issues occurred at the high-power conditions due to the rapid release of the high amount of hydrogen present in their a-Si films [48]. Additionally, the low iV_{oc} at the high-power conditions may also be related to a possible plasma damage on the thin interfacial layer during the a-Si film deposition.

To further investigate the impact of the power, the active phosphorus dopant profiles are measured using ECV after the $POCl_3$ diffusion, as shown in Fig. 1(c). In order to clearly present the doping profiles, the locations of all the interfacial oxide layers are referred to as zero. Within the doped-Si layers (left-hand side of the dash line), a higher power ($\geq$650 W) leads to a slightly lower doping concentration with less than 4×10^{19} cm^{-3}, while a doping concentration of around 5×10^{19} cm^{-3} is found for lower power ($\leq$500 W) conditions. The phosphorus doping profiles within the silicon substrate (right-hand side of the dash line) are similar for all the samples with the different PECVD deposition powers. It is interesting to observe that the ratios of the two stretching-mode peaks in the FTIR spectra are similar for all power conditions, as shown in Fig. 1(b). This indicates that the a-Si films deposited at different powers have similar film densities [43], which means the phosphorus atoms should have a similar diffusion coefficient in all the a-Si films. Thus, we would expect that the different power samples also have similar doping profiles within the doped-Si layer region. The slight difference observed in the measured doping profiles in the doped-Si layer region may be due to the blistering, which results in a faster etching rate during the ECV measurement. Thus, we conclude that low iV_{oc} for the low power (350 W) is probably due to the ineffective gas decomposition, while the low iV_{oc} values for the high power (650 and 800 W) are because of the blistering issues and possible plasma damages.

The contact resistivity values (ρ_c) of the doped-Si/SiO_x/Si structures, are added in red in Fig. 1(a). From the results, we find that the deposition power has a minor impact on the contact resistivity. We assume that the final contact resistivity with a similar thickness and doping concentration is mainly determined by the crystallinity of the doped silicon layer [26]. The crystallinity difference can be studied by the Raman spectroscopy, as shown in Fig. 1(d). As mentioned earlier, the sampling depth of the Raman laser is deeper than the thicknesses of the thin films, resulting in a weak a-Si peak, which is difficult to assess (around 480–510 cm^{-1}). Here, only the 500 W a-Si sample is used as a reference since all the a-Si samples have similar signals. After the thermal diffusion, the c-Si peak (around 520 cm^{-1}) becomes larger and wider than that of the a-Si samples. This is related to the crystallization of a-Si after the thermal diffusion process: polycrystalline or microcrystalline phases start appearing [possible contributed peak range is highlighted in Fig. 1(d)], which leads to wider peaks and the increase of the total crystalline phases leads to an increase in the peak intensity [49]. The intensity and width of the c-Si peak in the Raman measurements could represent the degree of crystallinity of the doped silicon films. From Fig. 1(d), we find that power has no significant impact on the crystallinity of the silicon films after the thermal diffusion process. As a result, the passivating contact structures fabricated by different powers have similar contact resistivity values of around 6 $m\Omega \cdot cm^2$, as indicated in Fig. 1(a). The slightly higher ρ_c value at 800 W is due to its thicker layer.

B. *Influence of Pressure*

It is worth mentioning that all of the silicon films deposited under the different PECVD pressures (at a power of 500 W) have no blistering issues before or after the thermal diffusion. The different deposition pressures have minor impacts on the iV_{oc} values of both as-deposited a-Si/SiO_x and their final passivating contacts, as shown in Fig. 3(a). A consistent low iV_{oc} of $\sim$640 mV is obtained for all silicon samples with a-Si/SiO_x deposited at a different pressure, which may be due to their lower hydrogen concentrations [comparing Fig. 3(b) with Fig. 1(b)] than that in the different power cases.

After the $POCl_3$ diffusion process, the iV_{oc} of 0.1 mbar pressure sample (719 mV) only has 2 mV lower than the samples of the two higher pressure conditions (721 mV), as shown in Fig. 3(a). From the ECV results in Fig. 3(c), under the condition of 0.1 mbar, the phosphorus concentrations in both the doped-Si layer and the silicon substrate are slightly higher than that of the two higher pressure cases (0.2 and 0.4 mbar). The corresponding film densities can be approximated by comparing the SiH_2/SiH band ratios from the FTIR spectra [38], as shown in Fig. 3(b). The bond ratios corresponding to the pressure conditions of 0.1 mbar, 0.2 mbar, and 0.4 mbar are 1.52, 1.27, and 1.30, respectively. After reaching 0.2 mbar, the ratio starts to saturate at $\sim$1.3. Thus, a larger ratio at 0.1 mbar indicates a low-density film with a high concentration of the microcavities [39] and on the other side, the high pressure ($>$0.2 mbar) is likely to produce the dense films with less microcavities. From the Raman measurements in Fig. 3(d), the peak intensity is significantly lower for the 0.1 mbar doped-Si layer than that of the other two higher pressure conditions. Combined with the results of our previous works [26], there seems to be a clear correlation between the film density and crystallinity. We suggest that the low density under the condition of 0.1 mbar may be caused by the low crystallinity. The 0.1 mbar doped-Si layer has a lower crystallinity and a higher silicon atom disorder, resulting in a decrease in the number of the silicon atoms per unit volume. We speculate that the higher phosphorus concentration might be due to the lower density of 0.1 mbar silicon layers. The lower film density facilitates more phosphorus atoms being incorporated in the silicon layers as well as being diffused into the silicon substrate.

In order to examine the impact of the doping profile in the silicon substrate on their final iV_{oc}, EDNA2 [50] simulations are used to calculate the recombination contribution of the

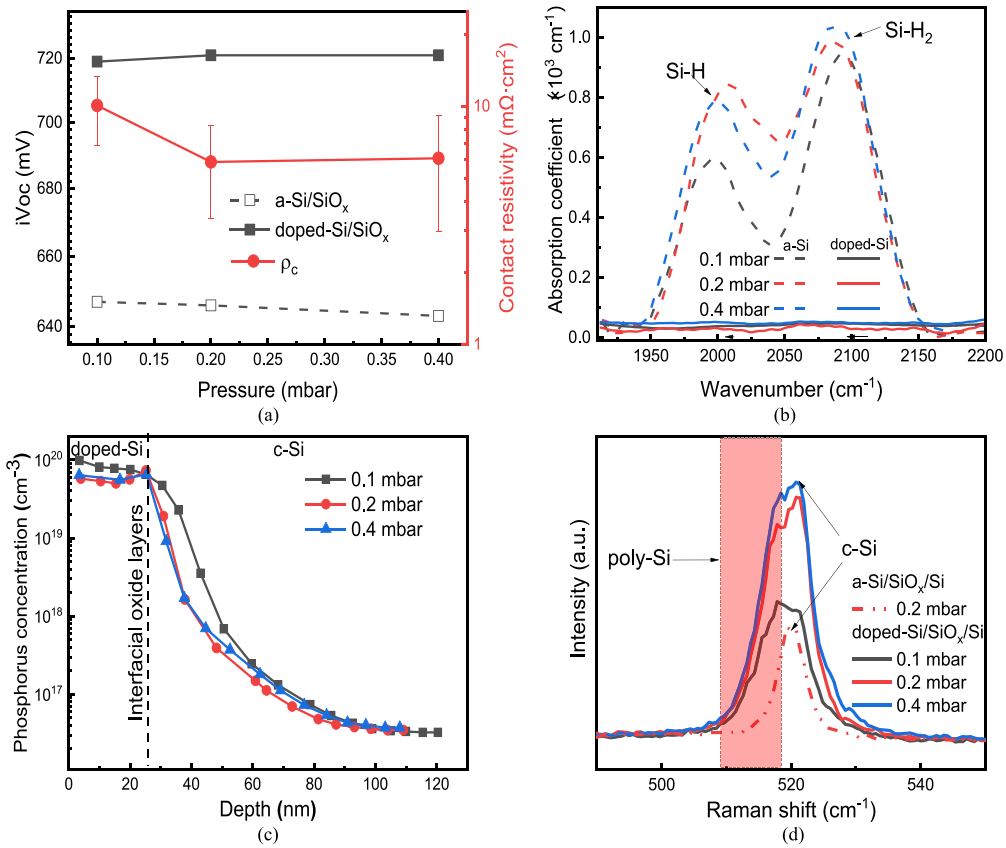

Fig. 3. Comparison of the electrical and material properties of a-Si (dashed lines, open symbols) deposited by different PECVD deposition pressures and corresponding doped-Si (solid lines, filled symbols). (a) Implied open-circuit voltage (black) and contact resistivity (red). (b) Detail view for the FTIR absorption coefficient peaks of Si-H and Si-H2. (c) ECV doping profile of the final doped-Si/SiO_x/Si structures. (d) Raman spectra of 500 W a-Si/SiO_x/Si together with the doped-Si/SiO_x/Si structures deposited at different pressures. The highlighted area is the range corresponding to the polycrystalline or microcrystalline phases' contributions.

different doping profiles. We assume no Shockley–Read–Hall recombination in the bulk of the highly doped region, just the Auger recombination. The simulated Auger recombination current densities ($J_{0.A}$) are 2.39 fA/cm^2, 1.41 fA/cm^2, and 1.40 fA/cm^2 for the dopant profiles of the 0.1 mbar, 0.2 mbar, and 0.4 mbar samples, respectively. Through adjusting the effective surface recombination velocity S_{eff} as 3790, 3760, and 3750 cm/s for different samples, the difference in the simulated $J_{0.A}$ values is consistent with the different recombination current densities J_0 of the passivating contact structures extracted from the PCD measurements [51]: 12 fA/cm^2, 9.81 fA/cm^2, and 9.65 fA/cm^2 corresponding to 0.1 mbar, 0.2 mbar, and 0.4 mbar, respectively. The higher doping concentration in the silicon substrate observed for the 0.1 mbar pressure condition results in a higher Auger recombination component and a higher J_0, thus explaining the slightly lower iV_{oc} value measured for this condition.

The contact resistivity is slightly higher for the 0.1 mbar sample, as shown in Fig. 3(a) (red line), which is due to its different film crystallinity, as well as film porosity. The change of the deposition pressure may lead to the different degrees of crystallinity in the as-deposited a-Si films [52], as well as the final doped-Si layers. As shown in the Raman measurements in Fig. 3(d), we find that the 0.1 mbar films have a low degree of crystallinity, which results in a high contact resistivity. The other two higher-pressures cases ($\geq$0.2 mbar) show high crystallinity, together with a low contact resistivity of $\sim$5.8 mΩ·cm^2.

IV. Conclusion

In order to further explore the influence of the PECVD deposition process on the doped-Si/SiO_x passivating contacts, we studied the films' properties and the electrical performance of their corresponding passivating contact structures as a function of the PECVD deposition power and pressure.

The deposition power has a major impact on the passivation quality of the final passivating contact structures and a minor effect on the contact resistivity. The lower iV_{oc} values are observed at both a low and a high power. For the high-power cases (650 and 800 W), the decrease in iV_{oc} can be explained by the blistering issues occurring and possible interface damage. For the low-power case (350 W), the main cause of the low iV_{oc} is the ineffective decomposition of SiH_4 during the deposition. An optimized iV_{oc} of 721 mV is achieved under a power condition of 500 W. Meanwhile, a consistently low ρ_c value of $\sim$6 mΩ·cm^2 is achieved for the whole range of the power explored since the power has a marginal impact on the density and crystallinity of the a-Si films and the corresponding doped-Si layers, which can be observed from the FTIR and Raman analysis.

The deposition pressure has an opposite impact to those of the power. Only a slightly lower iV_{oc} value (2 mV) is measured for the low-pressure condition (0.1 mbar), related to the lower a-Si film density compared with that achieved at higher pressures. We found that the lower density of the film is the main reason for the different phosphorous profiles obtained for that case. Meanwhile, the 0.1 mbar deposition pressure gives a higher contact resistivity due to its lower crystallinity. A consistent low contact resistivity of $\sim 5.8\ \mathrm{m\Omega \cdot cm^2}$ is achieved at the pressures above 0.2 mbar thanks to the a-Si films having a higher degree of crystallinity.

In conclusion, it is possible to control the passivation quality and the contact resistivity using the deposition power and the deposition pressure. The passivation quality is related to the amount of the incorporated hydrogen, together with the possible plasma damage on the interfacial oxide. On the other hand, the contact resistivity is related to the film crystallinity. Using an intermediate (500 W) PECVD deposition power at relatively high pressure ($\geq$0.2 mbar) is beneficial in achieving the well-performing passivating contacts in our situation.

We have achieved a good cell efficiency performance (24.7%) by using this method [17], and this detailed study based on PECVD can further help us to improve the electrical performance of this structure in the solar cell devices in the future.

ACKNOWLEDGMENT

The authors would like to thank the Department of Electronic Materials Engineering in ANU, providing the Raman and FTIR equipment. The ellipsometry at the Australian National Fabrication Facility is used for the thickness measurement.

REFERENCES

[1] Y. H. Kwark, R. Sinton, and R. M. Swanson, "SIPOS heterojunction contacts to silicon," in *Proc. IEEE Int. Electron Devices Meeting*, 1984, pp. 742–745.

[2] Y. Kwark, R. Sinton, and R. Swanson, "Low J° contact structures using sipos and polysilicon films," in *Proc. IEEE Photovolt. Spec. Conf.*, 1985, vol. 18, pp. 787–791.

[3] J.-Y. Gan and R. M. Swanson, "Polysilicon emitters for silicon concentrator solar cells," in *Proc. IEEE Conf. Photovolt. Spec.*, 1990, pp. 245–250.

[4] F. Feldmann *et al.*, "Tunnel oxide passivated contacts as an alternative to partial rear contacts," *Solar Energy Mater. Solar Cells*, vol. 131, pp. 46–50, 2014.

[5] D. L. Young *et al.*, "Carrier-selective, passivated contacts for high efficiency silicon solar cells based on transparent conducting oxides," in *Proc. IEEE 40th Photovolt. Spec. Conf.*, 2014, pp. 1–5.

[6] F. Feldmann, R. Müller, C. Reichel, and M. Hermle, "Ion implantation into amorphous Si layers to form carrier-selective contacts for Si solar cells," *Phys. Status Solidi Rapid Res. Lett.*, vol. 8, pp. 767–770, 2014.

[7] Y. Tao *et al.*, "730 mV implied Voc enabled by tunnel oxide passivated contact with PECVD grown and crystallized n+ polycrystalline Si," in *Proc. IEEE 42nd Photovolt. Specialist Conf.*, 2015, pp. 1–5.

[8] U. Römer *et al.*, "Ion implantation for poly-Si passivated back-junction back-contacted solar cells," *IEEE J. Photovolt.*, vol. 5, no. 2, pp. 507–514, Mar. 2015.

[9] J. Stuckelberger *et al.*, "Passivating electron contact based on highly crystalline nanostructured silicon oxide layers for silicon solar cells," *Solar Energy Mater. Solar Cells*, vol. 158, pp. 2–10, 2016.

[10] R. Peibst *et al.*, "Working principle of carrier selective poly-Si/c-Si junctions: Is tunnelling the whole story?" *Solar Energy Mater. Solar Cells*, vol. 158, pp. 60–67, 2016.

[11] G. Nogay *et al.*, "Interplay of annealing temperature and doping in hole selective rear contacts based on silicon-rich silicon-carbide thin films," *Solar Energy Mater. Solar Cells*, vol. 173, pp. 18–24, 2017.

[12] M. Nicolai, M. Zanuccoli, F. Feldmann, M. Hermle, and C. Fiegna, "Analysis of silicon solar cells with poly-Si/SiOx carrier-selective base and emitter contacts," *IEEE J. Photovolt.*, vol. 8, no. 1, pp. 103–109, Jan. 2018.

[13] G. Yang *et al.*, "Poly-crystalline silicon-oxide films as carrier-selective passivating contacts for c-Si solar cells," *Appl. Phys. Lett.*, vol. 112, 2018, Art. no. 193904.

[14] F. Feldmann *et al.*, "Charge carrier transport mechanisms of passivating contacts studied by temperature-dependent J-V measurements," *Solar Energy Mater. Solar Cells*, vol. 178, pp. 15–19, 2018.

[15] F. Feldmann *et al.*, "A study on the charge carrier transport of passivating contacts," *IEEE J. Photovolt.*, vol. 8, no. 6, pp. 1503–1509, Nov. 2018.

[16] F. Haase *et al.*, "Perimeter recombination in 25%-efficient IBC solar cells with passivating POLO contacts for both polarities," *IEEE J. Photovolt.*, vol. 8, no. 1, pp. 23–29, Jan. 2018.

[17] D. Yan *et al.*, "High efficiency n-type silicon solar cells with passivating contacts based on PECVD silicon films doped by phosphorus diffusion," *Solar Energy Mater. Solar Cells*, vol. 193, pp. 80–84, 2019.

[18] F. Feldmann, M. Bivour, C. Reichel, M. Hermle, and S.W. Glunz, "Passivated rear contacts for high-efficiency n-type Si solar cells providing high interface passivation quality and excellent transport characteristics," *Solar Energy Mater. Solar Cells*, vol. 120, pp. 270–274, 2014.

[19] S. Glunz *et al.*, "The irresistible charm of a simple current flow pattern-25% with a solar cell featuring a full-area back contact," in *Proc. 31st Eur. Photovolt. Solar Energy Conf. Exhib.*, 2015, pp. 259–263.

[20] N. Nandakumar *et al.*, "Approaching 23% with large-area monoPoly cells using screen-printed and fired rear passivating contacts fabricated by inline PECVD," *Prog. Photovolt.*, vol. 27, pp. 107–112, 2019.

[21] F. Haase *et al.*, "Laser contact openings for local poly-Si-metal contacts enabling 26.1%-efficient POLO-IBC solar cells," *Solar Energy Mater. Solar Cells*, vol. 186, pp. 184–193, 2018.

[22] D. Yan, A. Cuevas, J. Bullock, Y. Wan, and C. Samundsett, "Phosphorus-diffused polysilicon contacts for solar cells," *Solar Energy Mater. Solar Cells*, vol. 142, pp. 75–82, 2015.

[23] D. Yan, A. Cuevas, Y. Wan, and J. Bullock, "Passivating contacts for silicon solar cells based on boron-diffused recrystallized amorphous silicon and thin dielectric interlayers," *Solar Energy Mater. Solar Cells*, vol. 152, pp. 73–79, 2016.

[24] H. J. Park *et al.*, "Passivation quality control in poly-Si/SiO/c-Si passivated contact solar cells with 734 mV implied open circuit voltage," *Solar Energy Mater. Solar Cells*, vol. 189, pp. 21–26, 2019.

[25] Y. Morimoto *et al.*, "Influence of the existence of an underlying SiO_2 layer on the lateral solid-phase epitaxy of amorphous silicon," *J. Electrochem. Soc.*, vol. 141, pp. 188–192, 1994.

[26] W. Chen *et al.*, "Influence of PECVD deposition temperature on phosphorus doped poly-silicon passivating contacts," *Solar Energy Mater. Solar Cells*, vol. 206, 2020, Art. no. 110348.

[27] M. Stuckelberger, "Hydrogenated amorphous silicon: Impact of process conditions on material properties and solar cell efficiency," Ph.D. dissertation, Ecole Polytech Federale De Lausanne, Lausanne, Switzerland, 2014.

[28] M. M. de Jong, J. de Koning, J. K. Rath, and R. E. I Schropp, "Identification of various plasma regimes in very high frequency PECVD of amorphous and nanocrystalline silicon near the phase transition," in *Proc. 25th Eur. Photovolt. Solar Energy Conf. Exhib./5th World Conf. Photovolt. Energy Convers.*, 2010, pp. 3149–3151.

[29] G. V. Elzakker, "Hydrogenated amorphous silicon solar cells deposited from silane diluted with hydrogen," Ph.D. dissertation, Dept. Elect. Sustainable Energy, Delft University of Technol., Delft, The Netherlands, 2010.

[30] B. Demaurex *et al.*, "Low-temperature plasma-deposited silicon epitaxial films: Growth and properties," *J. Appl. Phys.*, vol. 116, 2014, Art. no. 053519.

[31] Y. Wan, "Highly transparent and highly passivating Silicon nitride for solar cells," Ph.D. dissertation, Aust. Nat. Univ., Canberra, ACT, Australia, 2014.

[32] G. Turban, Y. Catherine, and B. Grolleau, "Mass spectrometry of a silane glow discharge during plasma deposition of a-Si:H films," *Thin Solid Films*, vol. 67, pp. 309–320, 1980.

[33] L. Martinu and D. Poitras, "Plasma deposition of optical films and coatings: A review," *J. Vac. Sci. Technol. A, Vac. Surf. Films*, vol. 18, pp. 2619–2645, 2000.

[34] R. H. Cox and H. Strack, "Ohmic contacts for GaAs devices," *Solid-State Electron.*, vol. 10, pp. 1213–1218, 1967.

[35] U. Römer *et al.*, "Recombination behavior and contact resistance of n+ and p+ poly-crystalline Si/mono-crystalline Si junctions," *Solar Energy Mater. Solar Cells*, vol. 131, pp. 85–91, 2014.
[36] H. K. Asuha, O. Maida, M. Takahashi, and H. Iwasa, "Nitric acid oxidation of Si to form ultrathin silicon dioxide layers with a low leakage current density," *J. Appl. Phys.*, vol. 94, pp. 7328–7335, 2003.
[37] Y. Y. Ong, B. T. Chen, F. E. H. Tay, and C. Iliescu, "Process analysis and optimization on PECVD amorphous silicon on glass substrate," *J. Phys., Conf. Ser.*, vol. 34, pp. 812–817, 2006.
[38] M. Stuckelberger *et al.*, "Comparison of amorphous silicon absorber materials: Light-induced degradation and solar cell efficiency," *J. Appl. Phys.*, vol. 114, 2013, Art. no. 154509.
[39] D. E. Kane and R. M. Swanson, "Measurement of the emitter saturation current by a contactless photoconductivity decay method," in *Proc. 18th IEEE Photovolt. Spec. Conf.*, vol. 18, 1985, pp. 578–583.
[40] G. Choong *et al.*, "Measurements of Raman crystallinity profiles in thin-film microcrystalline silicon solar cells," *J. Phys. D, Appl. Phys.*, vol. 46, 2013, Art. no. 235105.
[41] J. V. Carpenter *et al.*, "Substrate-independent analysis of microcrystalline silicon thin films using UV Raman spectroscopy," *Phys. Status Solidi (B) Basic Res.*, vol. 254, 2017, Art. no. 1700204.
[42] Y. Wan, K. R. McIntosh, and A. F. Thomson, "Characterisation and optimisation of PECVD SiNx as an antireflection coating and passivation layer for silicon solar cells," *AIP Adv.*, vol. 3, 2013, Art. no. 032113.
[43] G. Amato *et al.*, "Hydrogen bonding in amorphous silicon with use of the low-pressure chemical-vapor-deposition technique," *Phys. Rev. B*, vol. 43, pp. 6627–6632, 1991.
[44] C. Manfredotti *et al.*, "Influence of hydrogen-bonding configurations on the physical properties of hydrogenated amorphous silicon," *Phys. Rev. B*, vol. 50, pp. 18046–18053, 1994.
[45] B. Hekmatshoar, D. Shahrjerdi, M. Hopstaken, K. Fogel, and D. K. Sadana, "High-efficiency heterojunction solar cells on crystalline germanium substrates," *Appl. Phys. Lett.*, vol. 101, 2012, Art. no. 032102.
[46] J. J. H. Gielis, P. J. van den Oever, B. Hoex, M. C. M. van de Sanden, and W. M. M. Kessels, "Real-time study ofa−Si:H/c−Si heterointerface formation and epitaxial Si growth by spectroscopic ellipsometry, infrared spectroscopy, and second-harmonic generation," *Phys. Rev. B*, vol. 77, 2008, Art. no. 205329.
[47] C. H. Seager and D. S. Ginley, "Passivation of grain boundaries in polycrystalline silicon," *Appl. Phys. Lett.*, vol. 34, pp. 337–340, 1979.
[48] A. Morisset *et al.*, "Highly passivating and blister-free hole selective polysilicon based contact for large area crystalline silicon solar cells," *Solar Energy Mater. Solar Cells*, vol. 200, 2019, Art. no. 109912.
[49] W. S. Yoo *et al.*, "Grain size monitoring of 3D Flash memory channel poly-Si using multiwavelength Raman spectroscopy," in *Proc. IEEE 14th Annu. Non-Volatile Memory Technol. Symp.*, 2014, pp. 1–4.
[50] K. R. McIntosh and P. P. Altermatt, "A freeware 1D emitter model for silicon solar cells," in *Proc. 35th IEEE Photovolt. Spec. Conf.*, 2010, pp. 2188–2193.
[51] J. Stuckelberger *et al.*, "Recombination analysis of phosphorus-doped nanostructured silicon oxide passivating electron contacts for silicon solar cells," *IEEE J. Photovolt.*, vol. 8, no. 2, pp. 389–396, Mar. 2018.
[52] J. Gope *et al.*, "Amorphous and nanocrystalline silicon made by varying deposition pressure in PECVD process," *J. Non-Crystalline Solids*, vol. 355, pp. 2228–2232, 2009.